TU/e EINDHOVEN UNIVERSITY OF TECHNOLOGY

High-performance small vertical-cavity lasers: a comparison of measured improvements in optical and current confinement in devices using tapered apertures

Citation for published version (APA):
Hegblom, E. R., Margalit, N. M., Fiore, A., & Coldren, L. A. (1999). High-performance small vertical-cavity lasers: a comparison of measured improvements in optical and current confinement in devices using tapered apertures. *IEEE Journal of Selected Topics in Quantum Electronics*, *5*(3), 553-560. https://doi.org/10.1109/2944.788418

DOI:
10.1109/2944.788418

Document status and date:
Published: 01/01/1999

Document Version:
Publisher's PDF, also known as Version of Record (includes final page, issue and volume numbers)

Please check the document version of this publication:

• A submitted manuscript is the version of the article upon submission and before peer-review. There can be important differences between the submitted version and the official published version of record. People interested in the research are advised to contact the author for the final version of the publication, or visit the DOI to the publisher's website.
• The final author version and the galley proof are versions of the publication after peer review.
• The final published version features the final layout of the paper including the volume, issue and page numbers.

Link to publication

General rights
Copyright and moral rights for the publications made accessible in the public portal are retained by the authors and/or other copyright owners and it is a condition of accessing publications that users recognise and abide by the legal requirements associated with these rights.

• Users may download and print one copy of any publication from the public portal for the purpose of private study or research.
• You may not further distribute the material or use it for any profit-making activity or commercial gain
• You may freely distribute the URL identifying the publication in the public portal.

If the publication is distributed under the terms of Article 25fa of the Dutch Copyright Act, indicated by the "Taverne" license above, please follow below link for the End User Agreement:

www.tue.nl/taverne

Take down policy
If you believe that this document breaches copyright please contact us at:

openaccess@tue.nl

providing details and we will investigate your claim.

Download date: 04. Oct. 2023

High-Performance Small Vertical-Cavity Lasers: A Comparison of Measured Improvements in Optical and Current Confinement in Devices Using Tapered Apertures

E. R. Hegblom, N. M. Margalit, A. Fiore, and L. A. Coldren, *Fellow, IEEE*

***Abstract*— We analyze the scaling characteristics of the optical and current confinement for three different vertical-cavity surface-emitting laser (VCSEL) structures with tapered apertures. The improvements in scaling have allowed devices with apertures <3 μm to have wall-plug efficiencies over 20% at output powers as low as 150 μW. The combination of low threshold (<200 μA), single modedness, and good wall-plug efficiency even at low output powers makes these devices excellent candidates for short distance (<1 m) interconnects within computers.**

***Index Terms*—Current spreading, oxide apertures, optical scattering, semiconductor lasers, surface-emitting lasers.**

I. Introduction

THE MANUFACTURE of relatively *large*, multimode vertical-cavity lasers for data links using multimode fiber is now commonplace. However, in the future, relatively *small* ($\sim$5 μm) vertical-cavity lasers may also become important for other applications such as board-to-board or chip-to-chip free-space optical interconnections or high-speed printing [1]. These applications require arrays of lasers with low power consumption and operating at output powers of 100–500 μW. In the case of free-space interconnections (or when multimode fiber is not used), one usually wants single-mode devices to reduce optical crosstalk and intermodal noise, and that generally means using small diameters $\sim$3 μm. But smaller lasers are not only desirable for single-mode operation. If properly scaled (constant $J_{\mathrm{TH}}, \eta_{\mathrm{EX}}$), the Peak wall-plug efficiency will be higher in smaller devices despite resistance increasing as $\sim$1/(aperture diameter) [2]. Also, this higher wall-plug efficiency will occur, as desired, at lower output powers. Properly scaled devices will also provide higher modulation bandwidths at lower drive power. However, to realize these improvements, one must overcome several obstacles to scaling device characteristics, namely, optical scattering losses, current spreading, carrier diffusion, and increased electrical and thermal resistance.

Although current spreading or carrier diffusion will raise the threshold in larger ($\sim$10-μm diameter) devices, optical scattering losses present a much greater barrier at smaller sizes because they not only lower the slope efficiency, but they also increase the threshold gain which, in turn, leads to higher lateral leakage currents. The excess loss generally turns on sharply [3], [4] (roughly as $\sim(1/R_d)^3$, where R_d is the device radius) and will have an exponentially greater effect on threshold. These losses have been dramatically reduced by confining the mode with apertures rather than etched pillars [4], [5]. Our previous work with thin apertures [6] and tapered apertures [7] has demonstrated further reductions in scattering loss.

Current spreading between the aperture and the active region and carrier diffusion within the barriers and quantum wells raise the threshold, but by themselves should not affect the slope efficiency due to the clamping of the carrier population in the active region. One might expect the unclamped voltage at the aperture to increase the current spreading above threshold and drop the slope efficiency, but an estimate of this increased spreading above threshold suggests it should not be significant even at diameters of 1 μm [8]. Even so, the contribution of current spreading to threshold is significant at much larger diameters. As will be described in the Appendix, other experimental evidence in this work supports this conclusion.

Use of dielectric apertures instead of etched mesas for current confinement has also improved the scaling of the electrical resistance so it varies approximately as $1/R_D$ instead of $1/R_D^2$ as for the etched pillar case (R_D is the device radius). Under this geometry, both the thermal and electrical resistance scale in a similar manner. This scaling implies that, at a constant current density, the temperature and voltage (above the diode drop) should actually *decrease linearly* with device radius. Unfortunately, due to the parasitics of current spreading and carrier losses, a constant output power density does not translate into a constant current density versus device size. Also, even if all these lateral leakage and scattering loss parasitics were removed, the scaling of the thermal and electrical resistance implies an optimum device radius for a given

Manuscript received November 25, 1998; revised May 28, 1999. This work was supported by the Air Force Office of Scientific Research.

E. R. Hegblom was with the Electrical and Computer Engineering Department, University of California at Santa Barbara, Santa Barbara, CA 93106 USA. He is now with Hewlett Packard, Santa Barbara, CA 93117 USA.

N. M. Margalit was with the Electrical and Computer Engineering Department, University of California at Santa Barbara, Santa Barbara, CA 93106 USA. He is now with New Access Communications, San Jose, CA 95131 USA.

A. Fiore and L. A. Coldren are with the Electrical and Computer Engineering Department, University of California at Santa Barbara, Santa Barbara, CA 93106 USA.

Publisher Item Identifier S 1077-260X(99)06950-6.

1077–260X/99$10.00 © 1999 IEEE

output power. (This will be examined further in Section V.) Nevertheless, we can conclude that, as the operating power is lowered (provided parasitic optical and current/carrier leakage are removed), smaller devices will be more efficient despite increased electrical and thermal resistance.

Increased resistance at smaller sizes is a limitation when one wants to drive vertical-cavity surface-emitting lasers (VCSEL's) directly from 3.3 V CMOS, and we expect the device resistance still could be improved with better control of the doping profile in the first few mirror periods. Nevertheless, single-mode devices with aperture openings of 2–3 μm, 20% wall-plug efficiency at 150 μW, and with low (154 μA) threshold still had a drive voltage under 2.5 V at 300-μW output power. One might also expect the increased resistance at smaller sizes to increase the high-frequency *RC* time constant. However, it is the parasitic capacitance of the aperture that will allow the radial current distribution to widen at higher frequencies and lower the dynamic resistance. Thus, at high speed, one is limited more by the vertical resistance to reach the oxide (in series with the source resistance) and the parasitic capacitance across the oxide and diode depletion region, rather than the lateral resistance from funneling current into the aperture. This difference in resistance at high and low frequencies is also needed to explain the *RC* parasitic observed in apertured intracavity contacted devices [9].

Having summarized all the major limitations to device scaling, the aim of the remainder of this paper is to quantify the improvements to the device scaling as we compare three VCSEL structures. In Section II, we overview the different structures. In Sections III and IV, we analyze not only the optical confinement for the tapered apertures, but also the electrical confinement. In Section V, we quantify how the resistance scaling and current confinement impact the wall-plug efficiency. Lastly, in the Appendix, we analyze the size dependence of the clamping of the spontaneous emission.

Although other studies have also shown the improvement in optical confinement by positioning apertures at the standing wave Nulls [10]–[12], this work quantifies the effects for tapered apertures which also depend on the gradient of the taper. In addition, this work goes further to quantify the improvement in current confinement (by comparing two different structures both with apertures at the Nulls) and how these improvements combine with the scaling of the electrical resistance to impact the wall-plug efficiency at lower powers and at sizes small enough to be single mode. While high wall-plug efficiencies of 50% [13] and 57% [14] at output powers of 1.3 and 3.3 mW, respectively, have been achieved in larger 7- and 5-μm diameter devices, the improvements being touted here are for smaller single-mode devices at lower powers where the scaling issues are much more important.

II. Summary of Device Structures

A general schematic for the VCSEL's discussed in this paper is shown in Fig. 1. All the structures are bottom-emitting VCSEL's with 18.5 bottom mirror periods, as shown schematically in Fig. 1. They all have the same calculated mirror transmission (0.7%) and the same number (three)

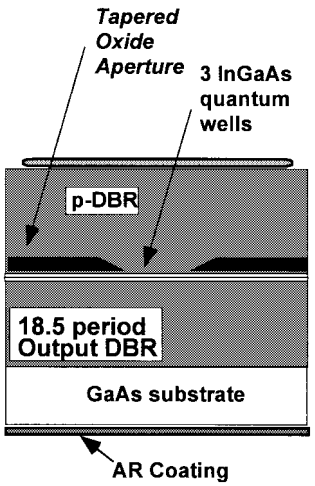

Fig. 1. General schematic for all three of the VCSEL structures discussed in this work.

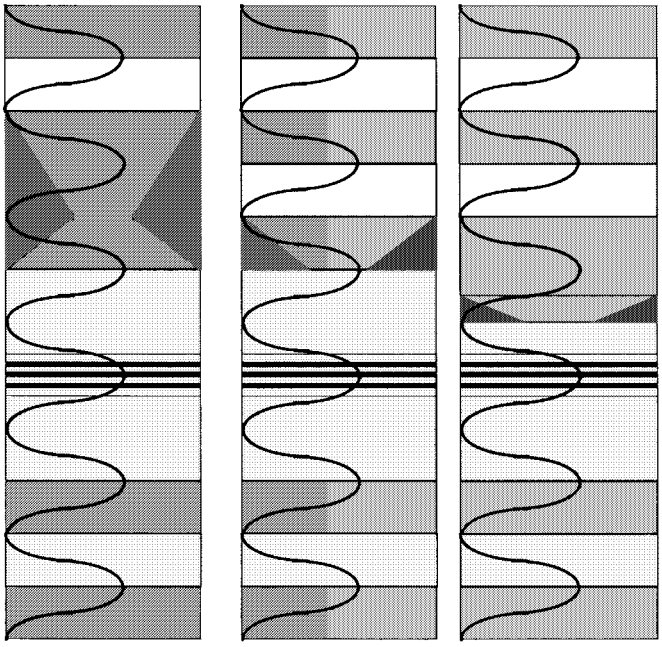

Fig. 2. Schematic of the central portion of three VCSEL structures discussed in this work in which the aperture is positioned at (a) the second Null from the active region, (b) the first Peak, and (c) the first Null. The black areas indicate the oxide aperture, the lightest regions represent GaAs, and the gray regions indicate AlGaAs, except for the three stripes across the center, which denote the three InGaAs QW active region. The oscillating line represents the standing-wave pattern. (Grading of the interfaces is not shown.)

and composition ($In_{0.18}Ga_{0.82}As$) for the quantum wells. A schematic of the central portion of the three different VCSEL structures examined in this paper are shown in Fig. 2(a)–(c). The aperture is centered at different points in the standing wave: the first Null from the active region, the first Peak, and the second Null. The distance between the aperture tip and the active region varies from $\sim$230 nm in the "second Null" device to $\sim$50 nm for the "first Null" device. All the tapers are created by oxidation of a thin AlAs layer adjacent to $Al_{0.9}Ga_{0.1}As$. For the first and second Null devices, the thin layer of AlAs is 10 nm thick and for the first Peak device the layer is 8.5 nm thick.

TABLE I
PARAMETERS FOR THE TAPERED APERTURE VCSEL'S UNDER INVESTIGATION

Aperture Position	2nd Null	1st Peak	1st Null
# Quantum Wells	3	3	3
Output Transmission	0.7%	0.7%	0.7%
Broad-Area Loss	0.12%/pass	0.37%/pass	0.10%/pass
J_{TH} (broad-area)	810A/cm^2	870A/cm^2	600A/cm^2
Est. doping between aperture and active	5e17 cm^{-3}	1e18 cm^{-3}	6e17 cm^{-3} (from SIMS)
Dist. between aperture and active	210nm	130nm	50nm
P-Dopant	Be	C	Be
N-Dopant	Si	Si	Si

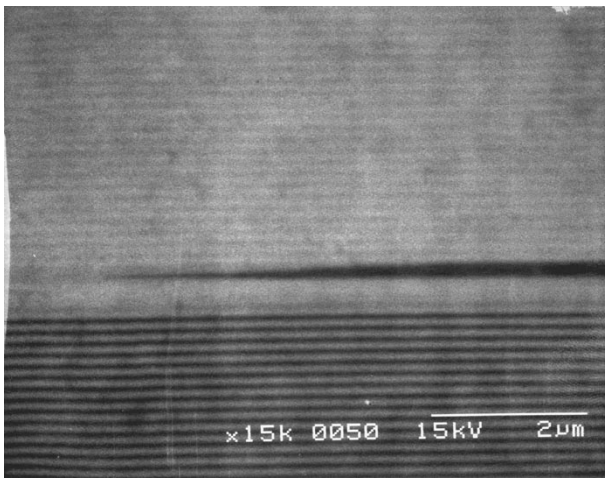

Fig. 3. SEM image of a laterally oxidized tapered aperture (black region).

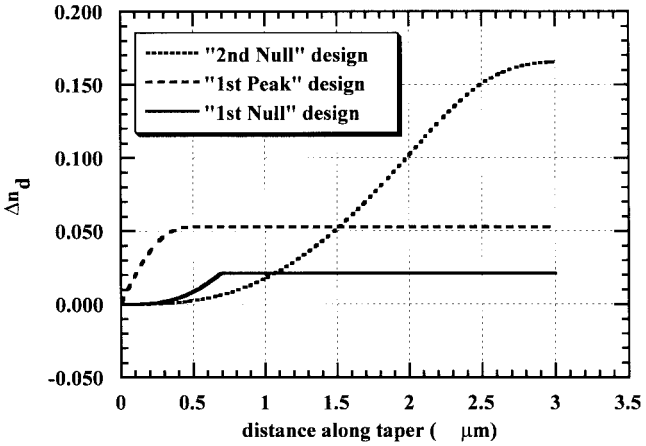

Fig. 4. Effective index step versus position for the three different taper aperture designs calculated assuming that the thickness varies linearly with position.

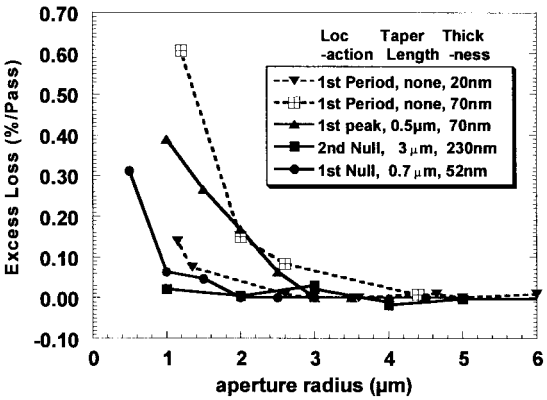

Fig. 5. Summary of the excess optical "scattering" loss extracted from the change in the slope efficiency with size for three tapered aperture devices and two other VCSEL's with abrupt apertures.

The first Peak and second Null devices are not intracavity contacted, and this impacts the broad-area slope efficiency because of some substrate absorption (but our comparison of scattering losses will not be affected). The first Peak device is carbon doped in the top mirror using a graphite filament in the molecular beam epitaxy (MBE) chamber. The top mirror in the second Null devices was Be doped and, aside from the aperture layer, it used an $Al_{0.7}Ga_{0.3}As$–GaAs top mirror as opposed to the other devices which used $Al_{0.9}Ga_{0.1}As$–GaAs top mirrors. (Unlike the first Null devices, the mirror in the second Null devices was grown entirely at 600 °C so the Be doping profile was far from ideal) Silicon doping was used in the bottom mirrors of all structures. Other details of the mirror doping and processing can be found in [7], [15], and [16]. Table I lists some of the different parameters. In the subsequent analysis, we will attempt to account for changes in the broad-area device parameters so that the scaling is the salient feature.

III. OPTICAL CONFINEMENT

For tapered apertures, the degree of optical confinement depends critically not only on the position of the aperture in the standing-wave, but also the gradient of the taper thickness which combine to give the gradient of the effective index step. From scanning election microscope measurements of the tapers (like that shown in Fig. 3), one can determine the taper length, though the exact taper profile is harder to determine. Nevertheless, we can estimate the index gradient if we assume the taper thickness varies linearly, and a plot of the effective index step Δn_d versus position is given in Fig. 4. The index step is calculated based upon the overlap of the index perturbation with the standing wave [17], which agrees with the index-step calculated based upon the change in the resonant wavelength [3], [17] except in the thickest regions where the perturbation of the oxide moves a second cavity resonance within the mirror stopband. One can see that the taper positioned at the standing-wave Peak has a much higher index gradient, and this results in increased scattering losses. These losses are plotted in Fig. 5. This excess optical loss is calculated by using the slope efficiency to extract the total optical loss and then subtracting the loss found in large (~20-μm diameter) devices [4], [5]. Calculating the total optical loss L_T (per pass)

$$L_T = \frac{T}{2}\left(\frac{T_s \eta_i}{\eta_{\text{ext}}} - 1\right) \tag{1}$$

relies upon calculating the output mirror transmission T, estimating the injection efficiency η_i, and the substrate transmission T_s, which was lower for the highly doped n-substrate under the "first Peak" VCSEL's. The substrate transmission can be directly measured by comparing the reflectivity in the stopband of the top of the distributed Bragg reflector (DBR) (effectively unity) with the reflectivity (again in the stopband) from the bottom of the sample. The injection efficiency is estimated to be 80% for the Be-doped devices and 90% for the "first-Peak" carbon-doped device. (The injection efficiency is consistently measured higher for carbon-doped in-plane lasers than for Be-doped in-plane lasers with the same structure presumably due to diffusing of the Be around the active region. This diffusion would increase the voltage to create inversion, and the corresponding excess field could lower the conduction band barrier that normally keeps electrons from entering the p-side.) One also would like to correct for any injection efficiency changes with size. Unfortunately, this is difficult to do. However, as mentioned, a theoretical estimate of the size dependence of the injection efficiency due to current leakage indicates an assumption of a constant injection efficiency is adequate, and the measurements in the Appendix suggest that this is correct. In addition, the excellent scaling of the slope efficiency of tapered apertured devices sets an upper bound on the drop of less than 10% at 2 μm. Despite this slight inaccuracy, our conclusions about the relative amounts of optical scattering from various aperture designs should be similar. We show the scattering loss in comparison to the theoretical preditcions from [3] in Fig. 6. Fig. 6(a) shows the comparison of the abrupt apertures data with the theoretical predictions and Fig. 6(b) shows the comparison for the tapered apertured devices. Comparison shows the measured loss is somewhat higher than predicted. Nevertheless, their coincidence on approximately the same scale suggests that scattering losses are significant in the devices and that the improvements observed agree with our understanding of optical loss. For the smallest size devices with tapered apertures, the comparison is trickier than for the abrupt apertures since it depends on the exact taper profile and the DBR stop-band. The second Null curve remains low and then curves up at the smallest sizes unlike the first Null curve. This effect has to do with the higher overall index step, which can confine smaller modes. (The mode radius for these sizes is predicted to be smaller than for the first Null curve.) The smaller modes at these sizes exceed the DBR angular stopband. The location of this rise is very sensitive to the taper length and the DBR angular stop band. The measured mode radius $(1/c^2)$ point for the second Null device at 1-μm radius was $\sim$1.5 μm, suggesting that the effective index may change more slowly around the aperture tip than estimated. The simulation for the first Null device suggests that, because of the weaker index step, the DBR angular stopband should not be creating excess loss at the 1- and 2-μm diameter openings, and this stipulation agrees with the measured mode size we describe below.

We can see from Fig. 5 that the first Peak apertures have only slightly lower scattering loss than for devices with an abrupt 80-nm-thick oxide aperture found in [18]. The taper is providing some benefit to decrease the loss, but it is clear

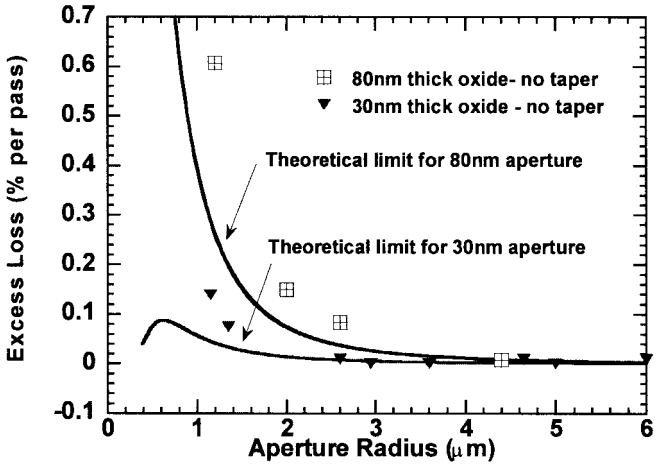

(a)

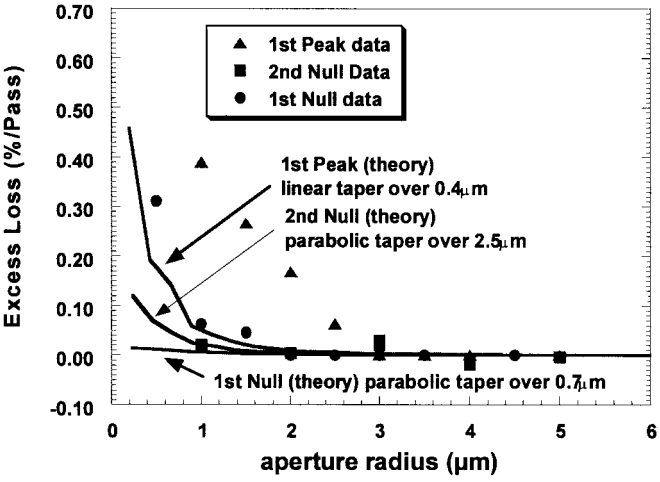

(b)

Fig. 6. Comparison of measured and predicated loss for the same structures as in Fig. 5 using calculations from [3] for (a) the abrupt apertures and for (b) the tapered apertures.

that the taper is more effective at standing-wave Nulls where the effective index gradient is lower. In fact, the excess loss is so low that the 2-μm-diameter second Null VCSEL was multimode. (The excess loss in the first Peak device is responsible for single-mode operation for the 2 and 3-μ-diameter devices because the waveguide index step of 0.06 is too strong to be a single-mode waveguide at that size.) On the other hand, the weaker waveguiding for the first Null device promoted single-mode operation for the 2- and 3-μm size devices. Optical spectra for the 3-μm first Null device is shown in Fig. 7.

The size given for the abrupt aperture devices from [6] and [18] in Fig. 5 is calculated based upon the lateral mode separation. The size for the aperture opening for the tapered aperture devices is determined by the closing of the aperture for pillars below a particular diameter. Since the pillar size increases in steps of 1 μm, a label of radius r_0 means the actual radius of the opening is between $r_0 - 0.5$ μm and r_0.

Due to the weaker guiding of both thinner apertures and tapered apertures, the mode is expected to be larger than the mode of an abrupt thick aperture of the same opening. Fig. 8

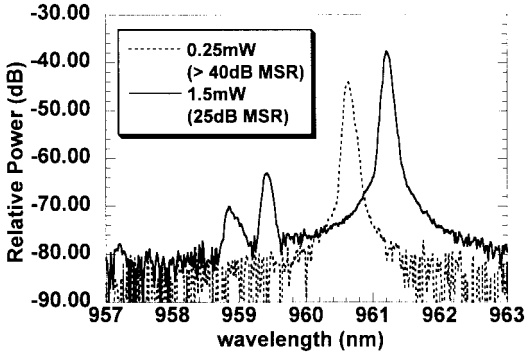

Fig. 7. Optical spectrum from a 3-μm first Null VCSEL showing single-mode operation at output powers below 1.5 mW.

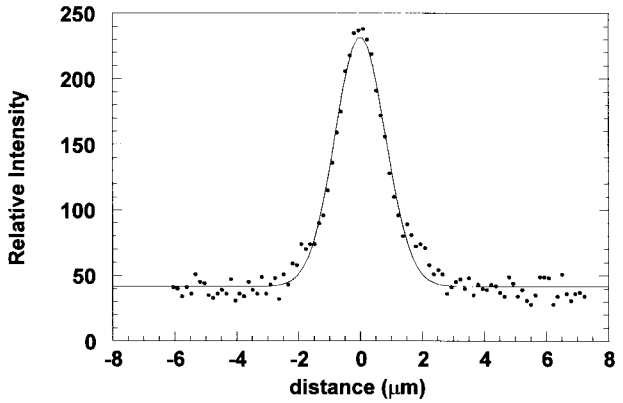

Fig. 8. Near-field intensity versus position for a mode from a first Null VCSEL with a 2-μm-diameter opening.

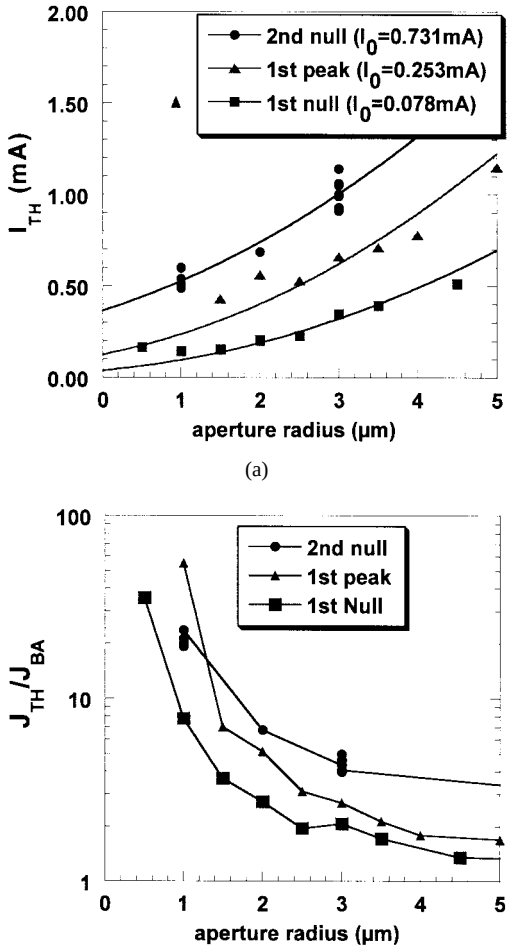

Fig. 9. (a) Threshold current versus aperture radius for three different taper designs. (b) Same data normalized by the broad-area threshold current density.

shows a line-scan of the near-field intensity in a first Null device with a 2-μm opening that shows about a $1/e^2$ diameter of 3 μm. The system resolution was not taken into account and, even though a high 0.75 NA lens was used, sharp features like the boundary of an etched mesa had a boundary about 1 μm wide. Thus, the actual diameter may be even smaller: approximately 2.8 $\mu\text{m} = \sqrt{(3\ \mu\text{m})^2 - (1\ \mu\text{m})^2}$. Based on a vertically uniform waveguide analysis, one can calculate that, for the mode guided by an 80-nm-thick abrupt aperture (effective index step, $\Delta n_d = 0.06$) to have a $1/e^2$ diameter of 3 μm, the radius of the aperture opening should be $\sim$1.8 μm. However, for this larger size, the excess optical losses of an abrupt 80-nm-thick aperture are around 0.2%/pass, which still is much greater than those for the 2- and 3-μm-diameter tapered and thin apertures. Thus, even at the same mode size, thin or tapered apertures are preferable to quarter-wave-thick ones. This result also agrees with theoretical calculations of the scattering loss versus mode size [3].

One may also ask if tapered apertures are preferable to thin apertures when both are placed near a standing-wave Null. From the point of view of optical scattering losses for the lowest order mode, there is little difference. However, there are situations where tapering is desirable. If one wishes to promote multimode operation in smaller VCSEL's, use of a thick tapered aperture is preferable to a thin aperture which will not guide higher order modes. Such a design is desired when making lower threshold "medium sized" ($\sim$5–10-μm diameter) VCSEL's for coupling to multimode fiber. Furthermore, tapering to greater thickness fairly far ($>$3 μm) from the optical mode is desirable to reduce the parasitic capacitance through the oxide. Finally, tapering may occur as a result of other design conditions. It is typically necessary to drive current through the layers within the aperture. Apertures at the first Null are within the cavity which is typically of high-index low-aluminum content. However, if there is a large discontinuity in the aluminum composition, then one can incur a high drive voltage. This can be avoided with longer grading or surrounding the aperture by higher aluminum content which will frequently create a tapered aperture. Therefore, one must be mindful of the index gradient to avoid higher loss.

IV. Current Confinement

With size-dependent optical losses nearly extinct, the next major challenge for improving the scaling of characteristics is to reduce the lateral current and carrier leakage. Previous studies have indicated that lateral current spreading between the aperture and the active region can be significant in apertured devices [4], [8], [10]. In Fig. 9(a), we plot the threshold current versus aperture radius for the three different structures. Although there is some difference in the broad-area threshold

current densities, most of the reduction in the threshold can be attributed to improved current confinement as the aperture is positioned closer to the active region. We see that even the close position of ~50 nm is still beneficial. For clarity, we have also plotted the ratio of the threshold current density to the broad-area threshold current density in Fig. 9(b). Although the first Peak devices have higher scattering losses, the increase in the QW threshold current is small (except at the smallest size) given the size of the active region. Therefore, most of the change in threshold current density relative to the broad-area threshold is due to current confinement only. To make this point clearer, it is useful to compare with the model developed in [8] for the spreading when there is a purely resistive region between the aperture and an active region with a diode *J–V* characteristic. In that model, $I_{\rm TH}$ (in the absence of excess loss) should scale as

$$I_{\rm TH} = J_{BA}\pi R^2 + \frac{I_0}{2} + R\sqrt{\pi J_{BA} I_0} \qquad (2)$$

where $I_0 = 8\pi(\eta kT/q)(t/\rho)$, for a layer of uniform resistivity ρ and thickness t.

Fig. 9(a) shows the fit we obtained for the parameter I_0, using the broad-area threshold current density from 20–30-μm-diameter devices. (For the first Peak device, we excluded the smallest size from the fit because the threshold current increases due to scattering losses.) Let us now compare the fitted I_0 parameter with that expected from the doping between the aperture and the active region. (Note that, for the fitted values, the dominant term in the threshold is $I_0/2$ for the smallest sizes.) With the thickest region between the aperture and the active region, the second Null devices show the highest I_0 as expected, but it is still almost four times higher than if the region were uniformly doped at $5 \cdot 10^{17}$ cm^{-3}—as approximately designed. One possible reason is that relatively low Be doping combined with movement during growth at the heterointerfaces creates a much higher vertical resistance forcing the current to spread further laterally. The carbon doped first Peak devices are a better example. These were doped around $1 \cdot 10^{18}$ cm^{-3} between the aperture and active region, which yields a predicted near expectation: I_0 ~0.2 mA (where a mobility ~60 cm^2/(V·s) is expected for the higher doping in AlGaAs). For the first Null device, we did not intentionally dope the region between the aperture and the active region, but SIMS of this region (which was grown at a substrate temperature of 600 °C) revealed that Be moved down during growth and reached a concentration of ~$6 \cdot 10^{17}$ cm^{-3} over this region. Using this value, we obtain $I_0 \sim 70$ μA, which is a reasonable match given the typical error in concentration and mobility.

An additional effect to briefly consider is that the injected profile actually matches the aperture size, in which case the injected current is smaller than the mode for the 2-μm device and the lateral confinement factor is 50%–70% (depending upon the true aperture size). However, this effect would only imply a factor of 1.4–2.4 higher threshold current density (assuming a logarithmic gain model with three QW's) needed in the active region, which is still well below the observed factor of ten. We should note that some reduction in the confinement factor is not detrimental and, in fact, can make for a lower threshold current than one would achieve for a unity confinement factor of a mode of the same size because the power density in the mode is not uniform.

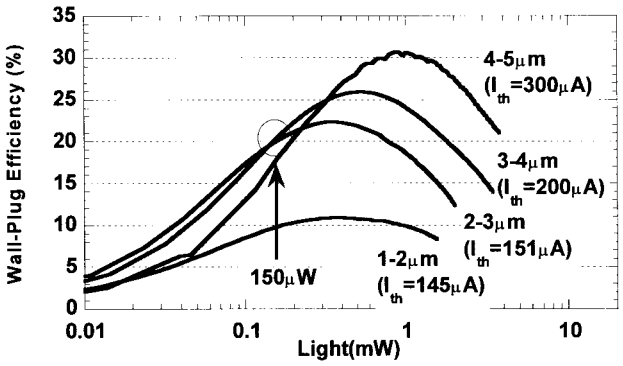

Fig. 10. Wall-plug efficiency versus output power for several first Null VCSEL's.

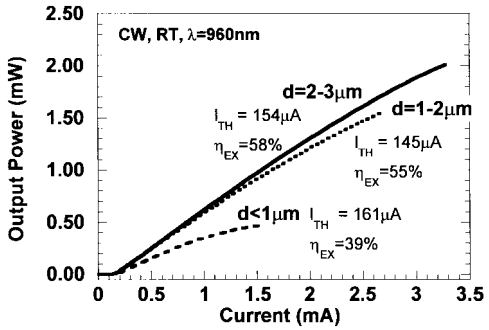

Fig. 11. *L–I* characteristics for the smallest of the first Null devices.

V. Scaling of Resistance and Wall-Plug Efficiency

In order to achieve high wall-plug efficiency at low output powers (100–500 μW), one desires even lower power dissipated at threshold. Consequently, one must be able to maintain high differential efficiency as the device threshold (and size) is reduced. With low background losses and scattering losses and improved current confinement, the first Null VCSEL's presented can provide high wall-plug efficiency at low output powers. Fig. 10 shows the wall-plug efficiency versus output power for several first Null devices described in this paper. The 4- and 3-μm-diameter devices have Peak wall efficiencies of 26% and 22% at output powers of 0.5 and 0.34 mW, respectively. Also, one slightly higher threshold device (5-μm device) reached 30% wall-plug efficiency at 0.9 mW. At 150 μW, the 3-μm device shown has a wall-plug efficiency of 20%. Fig. 11 shows the *L–I* curves for the smaller of these same devices. We see even that a 1-μm-diameter device (as discussed, 1 μm is the upper bound on the diameter) lases with a threshold of 161 μA and $\eta_{\rm EX} = 39\%$.

Although the threshold may be lower for smaller devices, the Peak wall-plug efficiency suffers because the devices have a resistance that increases approximately inversely with aperture radius (in agreement with other studies [2], [19]). Even if there was no current spreading, the increase in resistance causes the wall-plug efficiency (at a given output power) to

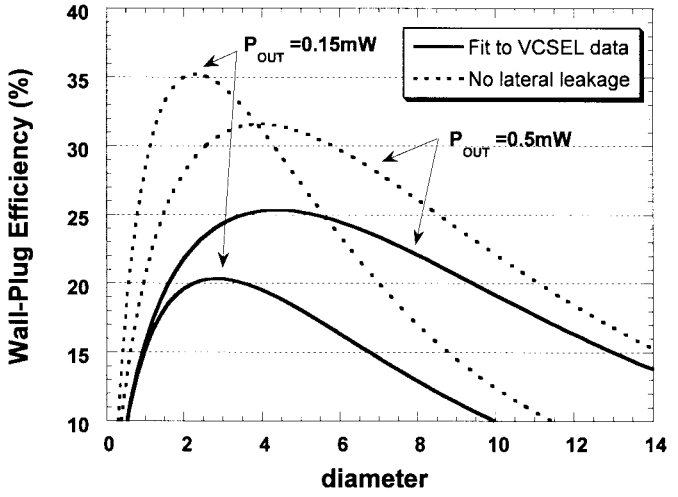

Fig. 12. Extrapolated wall-plug efficiency versus device size with and without lateral leakage currents.

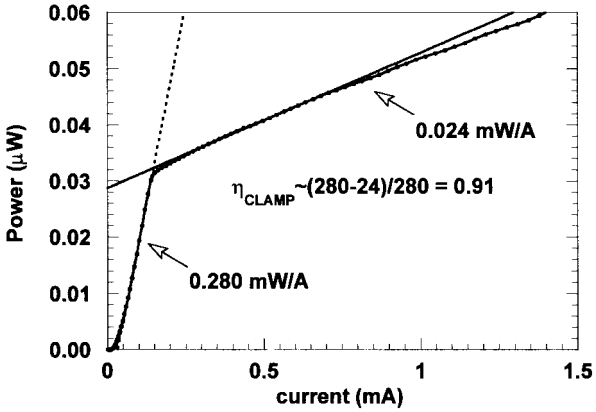

Fig. 13. Clamping of the spontaneous emission in a 3-μm-diameter first Null device.

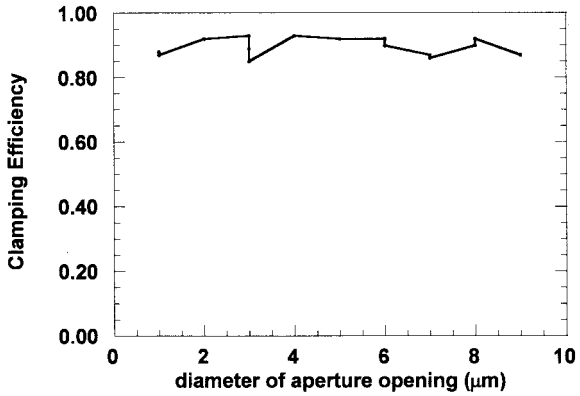

Fig. 14. Extracted "clamping" efficiency versus aperture size for the first Null devices.

have a maximum at a particular device diameter. However, as output power is lowered, removal of parasitic leakage becomes even more important for higher power conversion efficiency. In fact, if the resistance increases as 1/(aperture radius) and there is no lateral leakage or optical losses, then the Peak wall-plug efficiency will be higher in smaller devices. Of course, this Peak keeps occurring at lower and lower powers. If we resign ourselves to having leakage current, then it may be desirable to make a larger size device single mode. To illustrate these points, we have fit the size dependence of various device parameters of the first Null devices and in order to extrapolate to the condition of no lateral leakage current. Fig. 12 plots the wall-plug efficiency versus size at two different output powers of 0.5 and 0.15 mW based on the actual data and the case of no leakage current. As we see from the graph, when leakage is present the wall-plug efficiency at 0.5 mW is higher than at 0.2 mW, but if leakage is removed the efficiency is actually higher at 0.2 mW than at 0.5 mW. To generate the curves, both the size dependence of the *I–V* curves and the threshold current for the first Null devices was fit versus size and the slope efficiency was held constant (which only has a minor error at small sizes). The operating voltage fit to a current independent voltage V_D, which varied as $V_D = 1.49 + 0.745d^{-1.56}$ (volts), where d is the aperture diameter in μm, and a series resistance R_S, varying as $R_S = 2.51k\Omega(1/d)^{0.7}$. The size dependence of the threshold fit well to $I_{\rm TH} = 0.13\,{\rm mA} + J_{BA}\pi(d/2)^2$, where $J_{BA} = 600$ A/cm^2. (Also, the constant term was ignored to simulate no leakage current).

VI. Conclusion

This paper has examined the improvements in optical and current confinement and in wall-plug efficiency by varying the design and placement of tapered apertures in vertical-cavity lasers. These improvements in optical and current confinement are important for achieving higher power conversion efficiency at lower powers and smaller sizes where devices tend to be single mode and can be modulated faster with lower drive powers. Improvements in optical confinement have nearly eliminated optical scattering losses relative to typical background losses, and bringing the aperture within 50 nm of the active region still makes improvements in current confinement. These improvements have enabled small single-mode $<$3-μm-diameter devices with a threshold of 154 μA to reach 20% power conversion efficiency at output powers as low as 150 μW. Further improvement in current or carrier confinement will lead to even higher conversion efficiencies at smaller sizes and lower output powers.

Appendix
Scaling of the Clamping Efficiency

As previously discussed, we would like to have some idea of the scaling of the injection efficiency with size. One possible way to estimate this is to measure the clamping of the spontaneous emission. The thought here is that if carriers are moving laterally outside the region where they are "clamped," then this should show up as a relative increase in the spontaneous emission above threshold. To measure it, we placed a 930-nm bandpass filter in front of the detector and recorded the light versus current. At 930 nm, we are measuring emission from the upper states in the InGaAs quantum wells so we will not see carriers recombining in the barriers and cannot measure the total injection efficiency (by injection efficiency, we mean the above threshold injection

efficiency which multiplies the optical efficiency to yield the slope efficiency above threshold).

Fig. 13 shows the optical power of the spontaneous emission versus current for a 3-μm first Null VCSEL, and we observe the expected change in slope at threshold. Independent of any changes in optical coupling, we can calculate what we will call the clamping efficiency $\eta_c = (\eta_b - \eta_a)/\eta_b$, where η_a and η_b are the slope efficiencies of the spontaneous emission above and below threshold, respectively. Fig. 14 shows this clamping efficiency versus size. We see no strong variation with size which suggests that additional carriers injected above threshold going into unclamped regions relative to clamped regions changes negligibly with size. There are a number of assumptions which keep us from unequivocally concluding the lateral injection efficiency is not changing with size, but these data provide strong evidence that there is little variation laterally, which is in agreement with theoretical predictions [8]. Lastly, we should note that these measurements are on devices with low scattering losses. If one were to measure devices with high scattering losses, one might see a lowering of the *vertical* injection efficiency with size since the carrier density in the active region must rise with the additional loss.

However, these measurements beg other explanations for the small drop in efficiency at the smallest sizes. The other possible causes are the thermal rollover or an increase in optical losses. Part of the drop may also be accounted for by the mode becoming so small and divergent that collecting all the light in the detector is difficult. Estimates of the mode size and measurement with a larger detector indicate that this accounts for about a 2% drop in the efficiency which still does not explain the drop from 55% to 39% slope efficiency in the smallest device. But the sharp roll-over of the 1-μm-diameter device, even at a smaller power density than the 2-μm device, implies heating is responsible. (In theory, if leakage currents were removed, then the heating will be lower even at a constant power density.) Lastly, we should mention that if the mode does not spread out and is scaled below a $1/e^2$ diameter of 1 μm, then one can expect significant optical losses from roll-off in the DBR reflectivity at the high angles [3]. But the light at the angles $>16°$ for AlGaAs–GaAs DBR will be internally reflected the bottom of the substrate and will not contribute to an increase in the slope efficiency.

REFERENCES

[1] R. L. Thornton, "Vertical cavity lasers for printing," in *Proc. LEOS Summer Topical Meeting*, WC1 p. 71, 1997.

[2] K. L. Lear and R. P. Schneider, "Uniparabolic mirror grading for vertical cavity surface emitting lasers," *Appl. Phys. Lett.*, vol. 68, pp. 605–607, 1996.

[3] E. R. Hegblom, D. I. Babic, B. J. Thibeault, and L. A. Coldren, "Scattering losses from dielectric apertures in vertical cavity lasers," *IEEE J. Select. Topics Quantum Electron.*, vol. 3, pp. 379–389, Apr. 1997.

[4] B. J. Thibeault, E. R. Hegblom, Y. A. Akulova, P. D. Floyd, J. Ko, R. Naone, and L. A. Coldren, "Electrical and optical losses in dielectrically-apertured vertical-cavity lasers," in *Proc. SPIE Photonics West '97*, 1997, vol. 3003-12.

[5] B. J. Thibeault, T. A. Strand, T. Wipiejewski, M. G. Peters, D. B. Young, S. W. Corzine, L. A. Coldren, and J. W. Scott, "Evaluating the effects of optical and carrier losses in etched post vertical cavity lasers," *J. Appl. Phys.*, vol. 78, pp. 5871–5876, 1995.

[6] B. J. Thibeault, E. R. Hegblom, P. D. Floyd, R. Naone, Y. Akulova, and L. A. Coldren, "Reduced optical scattering loss in vertical-cavity lasers using a thin (300 Å) oxide aperture," *IEEE Photon. Technol. Lett.*, vol. 8, pp. 593–596, 1996.

[7] E. R. Hegblom, B. J. Thibeault, R. L. Naone, and L. A. Coldren, "Vertical cavity lasers with tapered oxide apertures for low scattering loss," *Electron. Lett.*, vol. 33, pp. 869–879, 1997.

[8] E. R. Hegblom, N. M. Margalit, B. J. Thibeault, L. A. Coldren, and J. E. Bowers, "Current spreading in apertured vertical cavity lasers," in *Proc. SPIE Photonics West*, 1997, vol. 3003, paper no. 23, pp. 176–179.

[9] B. J. Thibeault, K. Bertilsson, E. R. Hegblom, E. M. Strzelecka, Y. Akulova, and L. A. Coldren, "High speed characteristics of low optical loss oxide apertured vertical cavity lasers," *IEEE Photon. Technol. Lett.*, vol. 9, pp. 11–13, 1997.

[10] N. M. Margalit, J. Piprek, S. Zhang, D. I. Babic, K. Streubel, R. P. Mirin, J. R. Wesselmann, J. E. Bowers, and E. L. Hu, "64°C continuous-wave operation of 1.5 μm vertical cavity laser," *IEEE J. Select. Topics Quantum Electron.*, vol. 3, pp. 359–365, 1997.

[11] K. D. Choquette, W. W. Chow, G. R. Hadley, H. Q. Hou, and K. M. Geib, "Scalability of small-aperture selectively oxidized vertical cavity lasers," *Appl. Phys. Lett.*, vol. 70, pp. 823–825, 1997.

[12] A. E. Bond, P. D. Dapkus, and J. D. O'Brien, "Aperture placement effects in oxide-defined vertical cavity surface-emitting lasers," *IEEE Photon. Technol. Lett.*, vol. 10, pp. 1362–1363, 1998.

[13] K. L. Lear, K. D. Choquette, R. P. Schneider, S. P. Kilcoyne, and K. M. Geib, "Selectively oxidised vertical cavity lasers with 50% power conversion efficiency," *Electron. Lett.*, vol. 31, pp. 208–210, 1995.

[14] B. Weigl, M. Grabherr, C. Jung, R. Jager, G. Reiner, R. Michalzik, D. Sowada, and K. J. Ebeling, "High performance oxide-confined GaAs VCSEL's," *IEEE J. Select. Topics Quantum Electron.*, vol. 3, pp. 409–415, 1997.

[15] E. R. Hegblom, N. M. Margalit, A. Fiore, and L. A. Coldren, "Small, efficient vertical-cavity lasers with tapered oxide apertures," *Electron. Lett.*, vol. 34, pp. 895–897, 1998.

[16] E. R. Hegblom, R. L. Naone, N. M. Margalit, and L. A. Coldren, "Comparison of tapered apertures in vertical cavity lasers," in *Proc. LEOS '97*, 1997, vol. 2, no. ThI3, pp. 350–351.

[17] G. R. Hadley, "Effective index model for vertical-cavity surface-emitting lasers," *Opt. Lett.*, vol. 20, pp. 1483–1485, 1995.

[18] P. D. Floyd, B. J. Thibeault, E. R. Hegblom, J. Ko, and L. A. Coldren, "Comparison of optical losses in dielectric apertured vertical-cavity lasers," *IEEE Photon. Technol. Lett.*, vol. 8, pp. 590–592, 1996.

[19] K. L. Lear, H. Q. Hou, J. J. Banas, B. E. Hammons, J. Furioli, and M. Osinski, "Vertical cavity lasers on p-doped substrates," *Electron. Lett.*, vol. 33, pp. 783–784, 1997.

E. R. Hegblom, photograph and biography not available at the time of publication.

N. M. Margalit, photograph and biography not available at the time of publication.

A. Fiore, photograph and biography not available at the time of publication.

L. A. Coldren (S'67–M'72–SM'77–F'82), photograph and biography not available at the time of publication.